c. 2

NACA RM L50E26

NACA

RESEARCH MEMORANDUM

DAMPING IN ROLL OF RECTANGULAR WINGS OF SEVERAL ASPECT RATIOS AND NACA 65A-SERIES AIRFOIL SECTIONS OF SEVERAL THICKNESS RATIOS AT TRANSONIC AND SUPERSONIC SPEEDS AS DETERMINED WITH ROCKET-POWERED MODELS

By James L. Edmondson

Langley Aeronautical Laboratory
Langley Air Force Base, Va.

NATIONAL ADVISORY COMMITTEE FOR AERONAUTICS

WASHINGTON
August 24, 1950

UNCLASSIFIED

NATIONAL ADVISORY COMMITTEE FOR AERONAUTICS

RESEARCH MEMORANDUM

DAMPING IN ROLL OF RECTANGULAR WINGS OF SEVERAL ASPECT RATIOS AND NACA 65A-SERIES AIRFOIL SECTIONS OF SEVERAL THICKNESS RATIOS AT TRANSONIC AND SUPERSONIC SPEEDS AS DETERMINED WITH ROCKET-POWERED MODELS

By James L. Edmondson

SUMMARY

Rocket-powered flight tests have been conducted to determine the damping in roll of rectangular wings of various aspect ratios and thickness ratios with the use of the NACA 65A-series airfoil sections. The Mach number range of these tests was from approximately 0.8 to 1.4. The experimental damping in roll was consistently lower than that predicted by linear theory, and this difference increased with aspect ratio. The experimental damping in roll decreased as wing thickness ratio was increased.

An empirical correction factor dependent upon wing thickness ratio and aspect ratio was derived from the supersonic experimental results for use with existing supersonic linear theory to permit a more accurate prediction of the damping in roll of rectangular wings of finite thickness ratio. Further data are needed to determine the limits of operation for this factor.

INTRODUCTION

A damping-in-roll investigation has been conducted for a series of wings of several aspect ratios and airfoil thickness ratios using the NACA 65A-series airfoil section. Previous damping-in-roll tests of rectangular wings by this technique (reference 1) indicated that experimental damping would vary with airfoil thickness ratio; therefore, the present series of tests were conducted to determine the relationship between the damping in roll for both thickness ratio and aspect ratio.

The test wings were mounted on identical fuselages incorporating canted nozzles, as described in reference 1. The damping-in-roll coefficient and the total-drag coefficient were obtained for each configuration at zero lift through a Mach number range of approximately 0.8 to 1.4, corresponding to Reynolds numbers from 3×10^6 to 8×10^6. The models were tested in flight at the Pilotless Aircraft Research Station at Wallops Island, Va.

SYMBOLS

C_l	roll damping-moment coefficient (L/qSb)
C_{l_p}	damping-in-roll coefficient $\left(\dfrac{\partial C_l}{\partial \frac{pb}{2V}}\right)$
C_D	total-drag coefficient (D/qS)
D	total drag, pounds
L	roll damping moment, foot-pounds
L_p	rate of change of damping moment with rolling velocity, foot-pounds per radian per second
L_o	out-of-trim rolling moment, foot-pounds
T	torque, pound-foot
$\dot{\varphi}$, p	rolling angular velocity, radians per second
$\ddot{\varphi}$	rolling angular acceleration, radians per second^2
V	forward velocity, feet per second
q	dynamic pressure, pounds per square foot
M	Mach number
A	aspect ratio (b^2/S')
R	Reynolds number, based on wing chord
t/c	airfoil-section thickness ratio

d	body diameter, feet
b	wing span, feet (diameter of circle generated by wing tips)
S'	total wing area of two wings, square feet (wing panel assumed to extend to model center line)
S	total wing area of three wings, square feet (wing panel assumed to extend to model center line)
I_X	moment of inertia about longitudinal axis, slug-feet^2

Subscripts:

1	sustainer-on flight
2	coasting flight

MODEL AND APPARATUS

The models used in this investigation were identical to those reported in reference 1 except for wing design. The basic body consisted of a wooden fuselage containing a spinsonde nose section (reference 2) and using a sustaining rocket motor with canted nozzles. The test wings were attached near the rear of this basic fuselage in a three-wing arrangement. Wing aspect ratios of 2.5, 3.0, 3.7, and 4.5 using the NACA 65A009 airfoil section and airfoil thickness ratios of 0.06, 0.09, and 0.12 on wings of aspect ratio 3.7 were tested. A sketch of the model configuration and pertinent wing geometry are given in figure 1.

The models were boosted from a rail launcher to a Mach number of approximately 0.8, allowed to separate from the booster, then accelerated to a Mach number of approximately 1.4 by the internal rocket motor with canted nozzles. Therefore, these tests cover a Mach number range of about 0.8 to 1.4, corresponding to Reynolds numbers of 3×10^6 to 8×10^6, as shown in figure 1.

The rolling velocity and rolling acceleration were obtained by the modified spinsonde (reference 2) mounted in the nose of the model. The flight-path velocity and longitudinal acceleration were obtained with a Doppler radar velocimeter. Atmospheric data covering the altitude range of the flight tests were obtained with radiosondes.

REDUCTION OF DATA

The damping-in-roll derivative was calculated by balancing of moments acting on the model. The torque nozzle and wing out of trim produced rolling moments which were balanced by the moment of inertia and the damping moment produced by the wing and body. Moment equilibrium for one degree of freedom may be written

$$I_X\ddot{\varphi} - L_p\dot{\varphi} = T \pm L_o \tag{1}$$

Resolving equation (1) into coefficient form at the same Mach number for the accelerated and the decelerated portions of flight and solving them simultaneously for damping in roll yields

$$-C_{l_p} = \frac{\frac{T}{q_1} - \left(\frac{I_{X_1}\ddot{\varphi}_1}{q_1} - \frac{I_{X_2}\ddot{\varphi}_2}{q_2}\right)}{\frac{Sb^2}{2}\left(\frac{\dot{\varphi}_1}{V_1} - \frac{\dot{\varphi}_2}{V_2}\right)} \tag{2}$$

The complete analysis of this method for determining damping in roll may be found in reference 1.

The accuracy of C_{l_p}, C_D, and their component errors for these tests are within the following estimated limits:

Torque, T	±2.50
Rolling angular velocity, $\dot{\varphi}$	±1.00
Damping-in-roll coefficient, C_{l_p}	±0.04
Total-drag coefficient, C_D	±0.002
Mach number, M	±0.010

The preceding estimations are based on individual model calculations. However, the relative magnitudes of lateral trim change between duplicate models may affect the repeatability of $\dot{\varphi}$ and consequently C_{l_p} through the Mach numbers at which this trim change is effective. An analysis of other factors producing an error in C_{l_p} is reported in reference 1.

RESULTS AND DISCUSSION

The aspect-ratio series consists of models 1, 2, 3, and 4, and the thickness-ratio series consists of models 3, 5, and 6 (fig. 1). The experimental data for models 1, 2, 4, and 5 are presented herein; models 3 and 6 were reported in reference 1 and the results are repeated herein for comparison.

The rate of roll for models 1, 2, 4, and 5 is plotted against Mach number in figures 2(a), 2(b), 2(c), and 2(d), respectively. For models 2 and 5, for which records of duplicate models are shown, the difference in rate of roll with sustainer on was caused by a difference in torque produced by the canted nozzles. The rate-of-roll variation or lateral trim change through the transonic speeds during coasting flight has been discussed in reference 3. The severity of this lateral trim change seems to vary directly with wing thickness. An apparent discrepancy in rate of roll at $M \approx 0.93$ during sustainer-on flight is noted in figure 2(b). This discrepancy is the result of (1) the short time to record data and (2) the lateral trim change which is caused by local flow conditions dependent upon airfoil section and surface conditions (reference 3).

The variations of experimental C_{l_p} with Mach number are shown in figure 3. Also shown are supersonic theoretical curves of C_{l_p} from reference 4. This theory was derived for an isolated wing; however, the interference effects of a body and three wings are considered small through the body diameter-to-wing span ratios and Mach numbers of these tests. This has been shown by unpublished C_{l_p} data of wing alone, body plus two wings, and body plus three wings using wing plan form and body of model 3. Figures 3(a), 3(b), and 3(c) present the damping for the aspect-ratio series and show that the experimental curves are consistently lower in magnitude than theory. This difference between experiment and theory, however, varied directly with aspect ratio; the larger aspect ratios show a greater difference. Figure 3(b) shows the effect of the lateral trim change to be an apparent increase or decrease in damping, depending upon the relative magnitudes and direction of this trim change.

Figure 3(d) shows the damping for one of the thickness-ratio series; the other thickness-ratio models were reported in reference 1. A comparison of these thickness-ratio tests showed that the damping in roll varied inversely with wing thickness ratio; the greater thicknesses showed the less damping in roll.

The effects of aspect ratio and thickness ratio on damping in roll are summarized in the following table:

A	NACA airfoil section	$-C_{l_p}$ at M = 1.15	$-C_{l_p}$ at M = 1.30
2.5	65A009	0.255	0.283
3.0	65A009	.318	.325
3.7	65A009	.385	.363
4.5	65A009	.440	-----
3.7	65A012	.354	-----
3.7	65A006	.418	.405

An empirical correction factor which relates these experimental data with theory was derived to be used with existing supersonic linear-theory to allow prediction of C_{l_p} for wings of various thickness ratios. This factor, to be multiplied by values from supersonic linear theory, was found to be dependent upon wing aspect ratio as well as airfoil thickness ratio and is expressed as $\left(1 - \frac{t}{c}\right)^{2A/3}$.

The comparison of experimental C_{l_p} with corrected theoretical C_{l_p} for the thickness-ratio series is shown in figure 4(a). The solid curves are the corrected theory for the various thickness ratios. The thickness ratio of zero makes the correction factor equal to unity; therefore, this curve is the same as uncorrected linear theory. Experimental C_{l_p} is shown as dashed lines. These curves are the faired values from figure 3(d) of this paper and figure 9 of reference 1. Heretofore, the experimental curves for all these thickness ratios were compared to uncorrected theory shown as zero thickness ratio. It can readily be seen that the use of this empirical correction factor allows a much closer theoretical prediction of C_{l_p} for these test wings.

The agreement of the corrected theory with experimental data for the aspect-ratio series is shown in figure 4(b). Again, the corrected theory is shown as a solid curve for each aspect ratio, and experimental data for these aspect ratios are shown as dashed lines. The comparison of experimental C_{l_p} with uncorrected theory has previously been shown in figures 3(a), 3(b), and 3(c) of this paper and figure 9(a) of reference 1. The use of the empirical correction factor allows a much closer prediction of C_{l_p} for this range of aspect ratio.

Tests of a rectangular wing of aspect ratio 4.5 and NACA 65-006 airfoil section (reference 5) also showed good agreement with corrected theory. However, tests of double-wedge airfoil-section wing from references 5 and 6 show good agreement with supersonic linear theory above $M \approx 1.25$ without using a thickness correction factor. It is thus indicated that this factor will apply to a rounded-nose, smooth-contour airfoil of these wing-body combinations; however, additional data will be needed to determine the limits of operation.

The total-drag coefficients of these configurations were also obtained from these tests. The C_D are directly comparable because the wing area was constant in all cases. The relative effects of thickness ratio and aspect ratio on total drag are shown in figure 5. All configurations had approximately the same drag at subsonic speeds. At supersonic speeds the effect of increasing aspect ratio was a small increase in drag. However, as would be expected, the effect of increasing wing thickness ratio was to cause an earlier transonic drag rise and an appreciable increase in supersonic drag.

CONCLUSIONS

The following conclusions were drawn from tests of rectangular wings having NACA 65A-series airfoil sections, aspect ratios from 2.5 to 4.5, and thickness ratios from 0.06 to 0.12:

1. Damping in roll increased with increasing aspect ratio but at a slower rate than predicted by linear supersonic theory.

2. Damping in roll decreased with an increase in thickness ratio.

3. An empirical relationship factor was established which, when applied to linear theory, allows an accurate prediction of the damping in roll at supersonic speeds for the cases investigated.

Langley Aeronautical Laboratory
National Advisory Committee for Aeronautics
Langley Air Force Base, Va.

REFERENCES

1. Edmondson, James L., and Sanders, E. Claude, Jr.: A Free-Flight Technique for Measuring Damping in Roll by Use of Rocket-Powered Models and Some Initial Results for Rectangular Wings. NACA RM L9I01, 1949.

2. Harris, Orville R.: Determination of the Rate of Roll of Pilotless Aircraft Research Models by Means of Polarized Radio Waves. NACA TN 2023, 1950.

3. Stone, David G.: Wing-Dropping Characteristics of Some Straight and Swept Wings at Transonic Speeds as Determined with Rocket-Powered Models. NACA RM L50C01, 1950.

4. Harmon, Sidney M.: Stability Derivatives at Supersonic Speeds of Thin Rectangular Wings with Diagonals ahead of Tip Mach Lines. NACA Rep. 925, 1949.

5. Dietz, Albert E., and Edmondson, James L.: The Damping in Roll of Rocket-Powered Test Vehicles Having Rectangular Wings with NACA 65-006 and Symmetrical Double-Wedge Airfoil Sections of Aspect Ratio 4.5. NACA RM L50B10, 1950.

6. Brown, Clinton E., and Heinke, Harry S., Jr.: Preliminary Wind-Tunnel Tests of Triangular and Rectangular Wings in Steady Roll at Mach Numbers of 1.62 and 1.92. NACA RM L8L30, 1949.

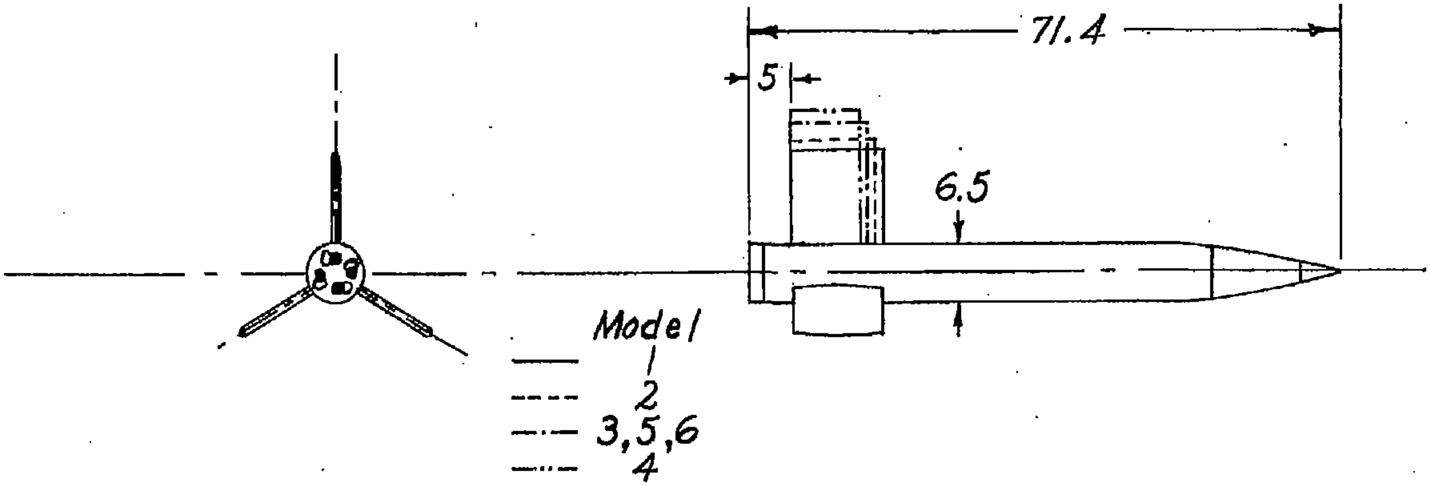

Model number	A	c	b/2	d/b	NACA airfoil section	R
1	2.5	11.193	13.992	.232	65A009	4.5 to 7.4 x 10^6
2	3.0	10.218	15.327	.212	65A009	4.1 to 7.2
3	3.7	9.192	17.039	.191	65A009	3.8 to 7.6
4	4.5	8.343	18.772	.173	65A009	3.3 to 5.5
5	3.7	9.192	17.039	.191	65A012	3.8 to 6.0
6	3.7	9.192	17.039	.191	65A006	3.8 to 7.8

Figure 1.- Sketch and wing geometry for the model tested. All dimensions in inches.

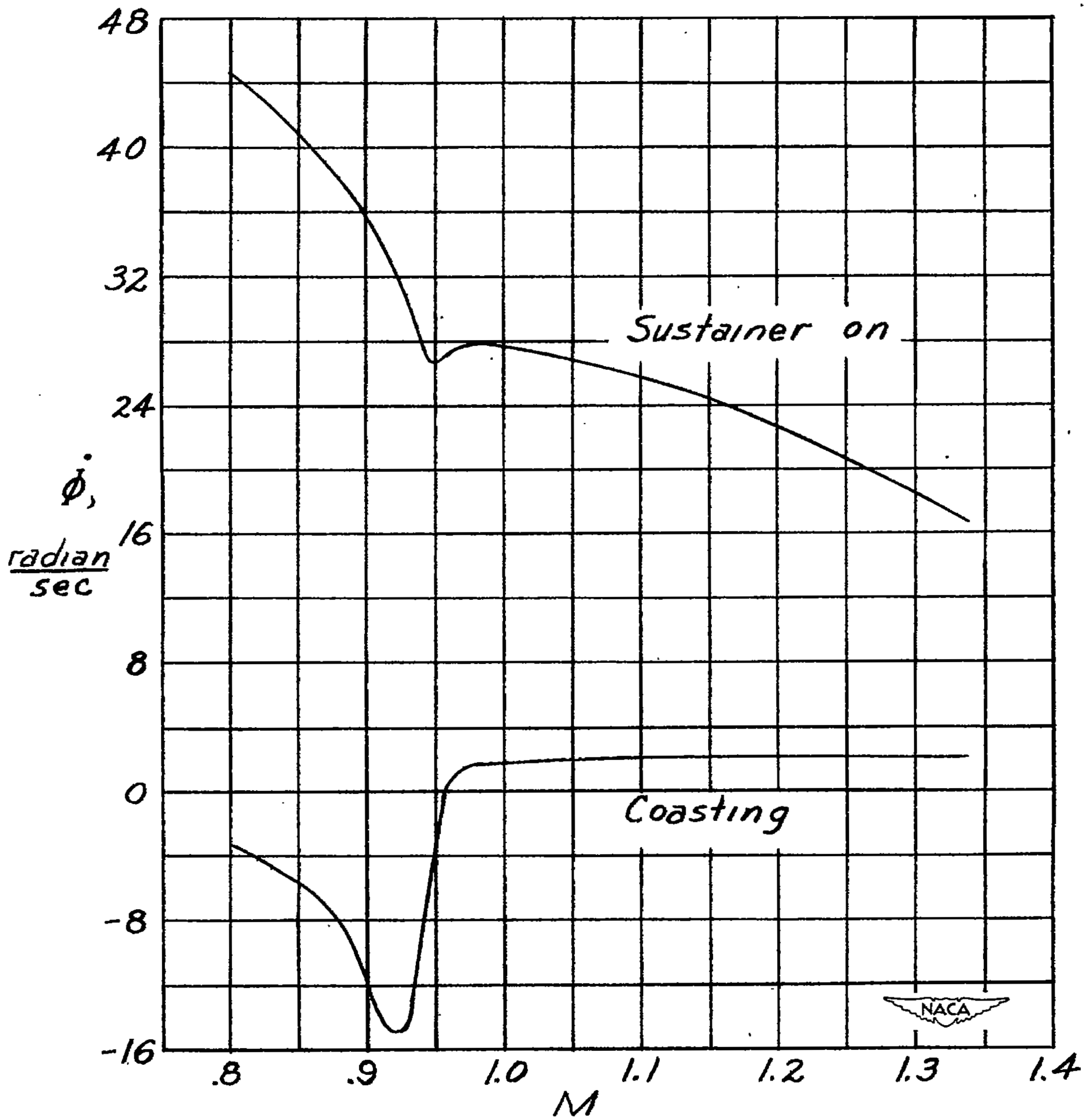

(a) Model 1; A = 2.5; $\frac{t}{c}$ =-0.09.

Figure 2.- Variation of rolling velocity with Mach number.

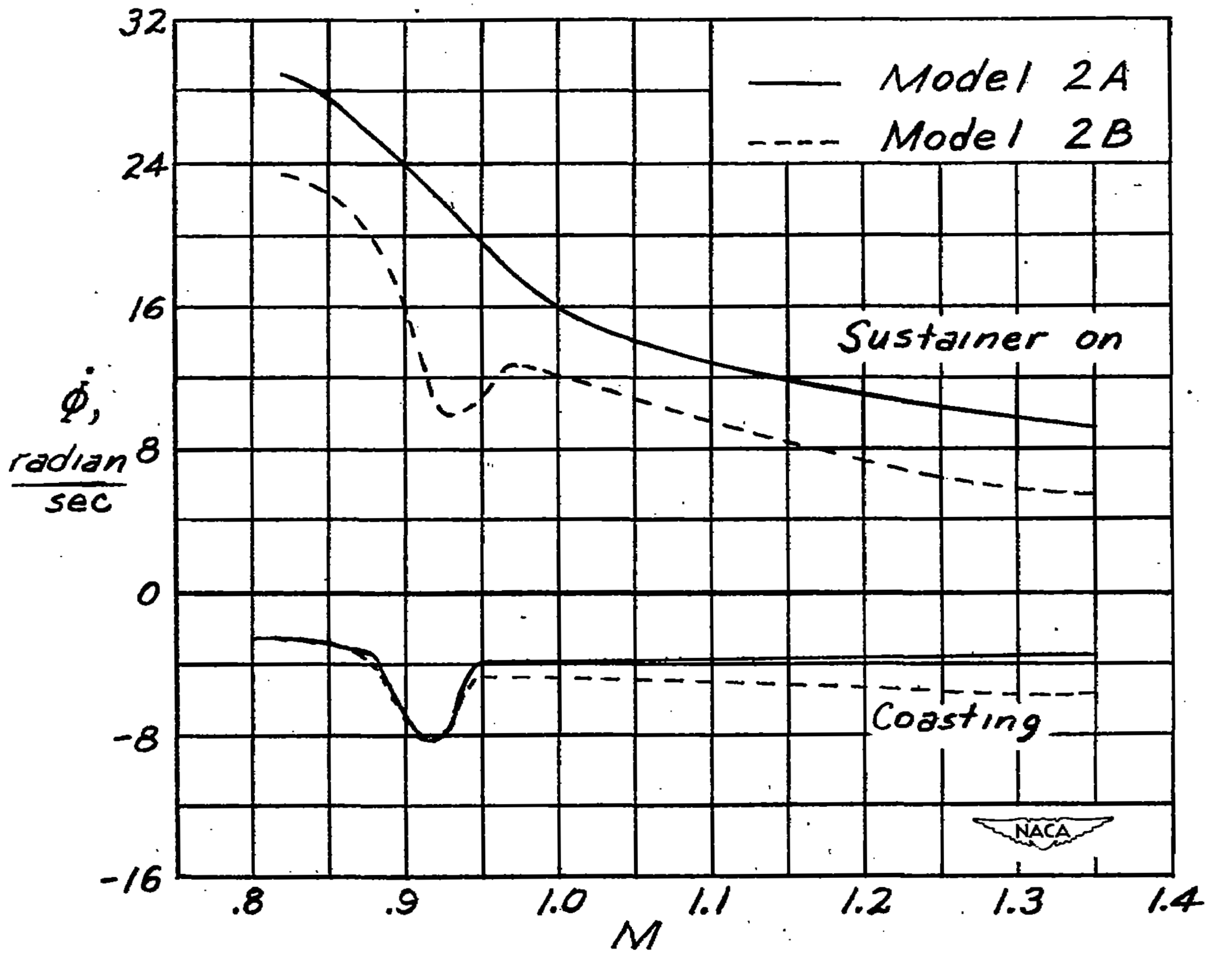

(b) Model 2; A = 3.0; $\frac{t}{c}$ = 0.09.

Figure 2.- Continued.

[redacted]

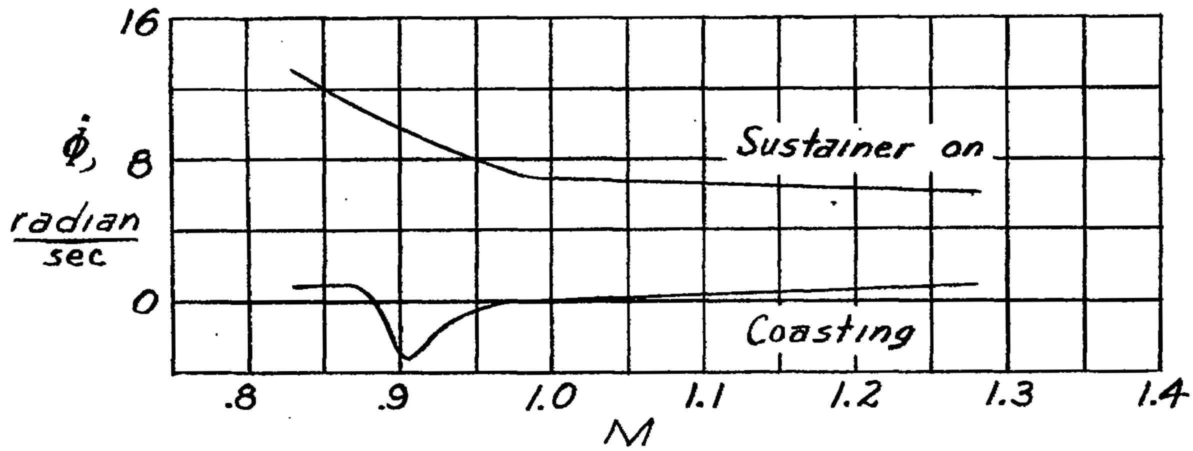

(c) Model 4; A = 4.5; $\frac{t}{c}$ = 0.09.

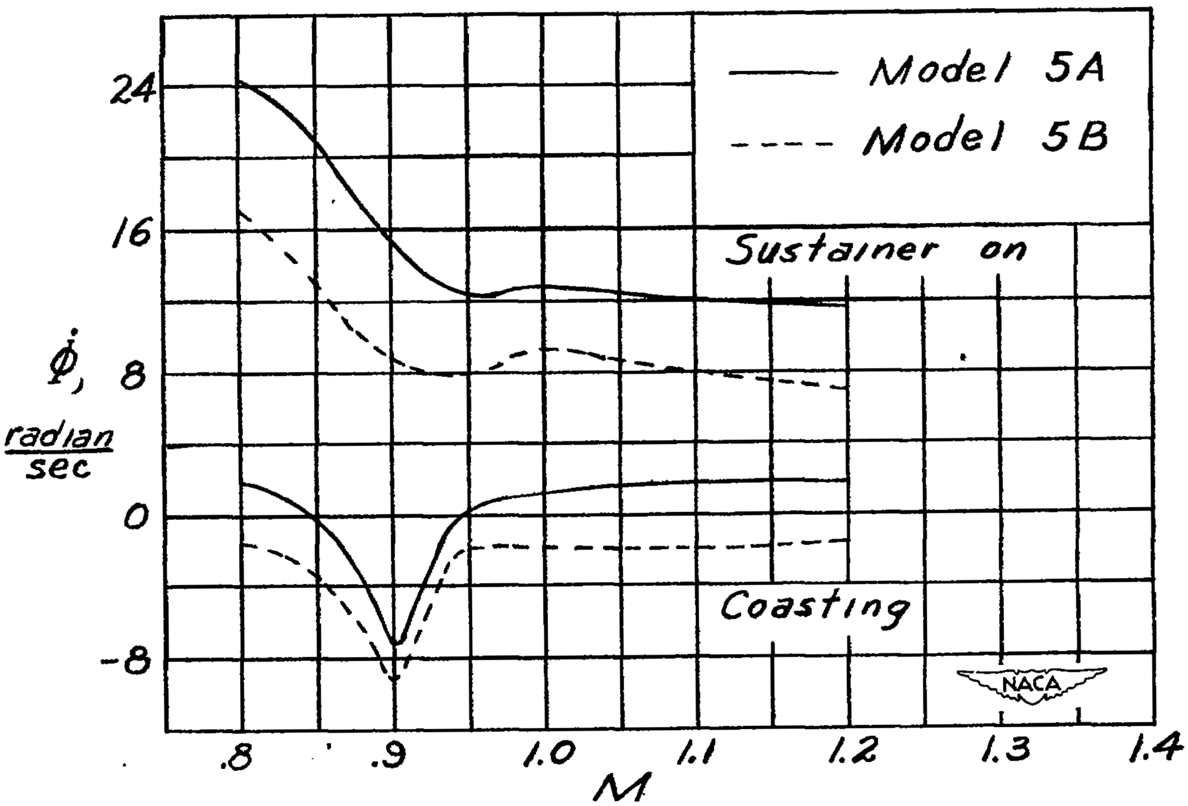

(d) Model 5; A = 3.7; $\frac{t}{c}$ = 0.12.

Figure 2.- Concluded.

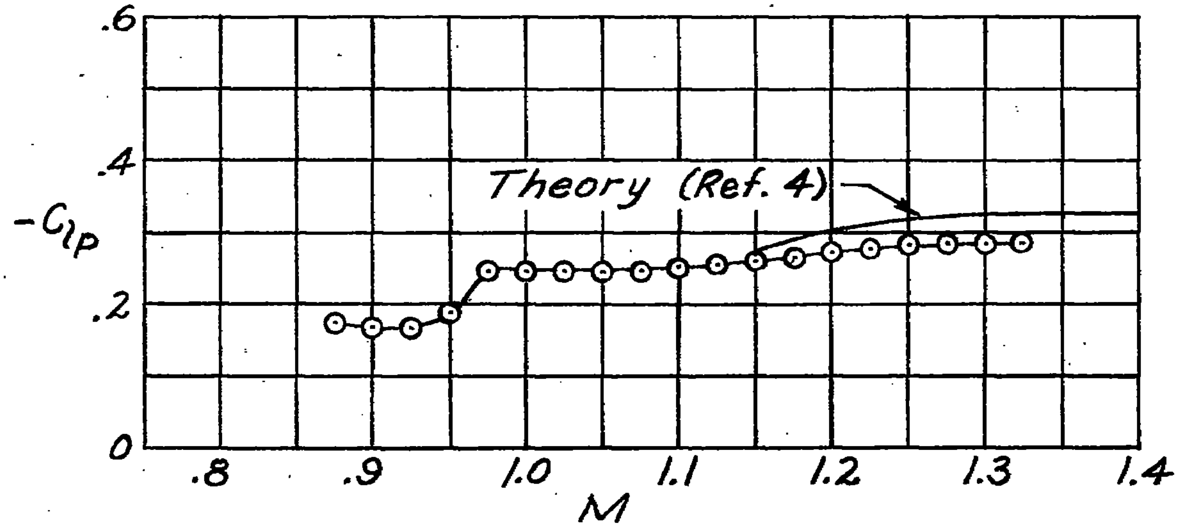

(a) Model 1; A = 2.5; $\frac{t}{c}$ = 0.09.

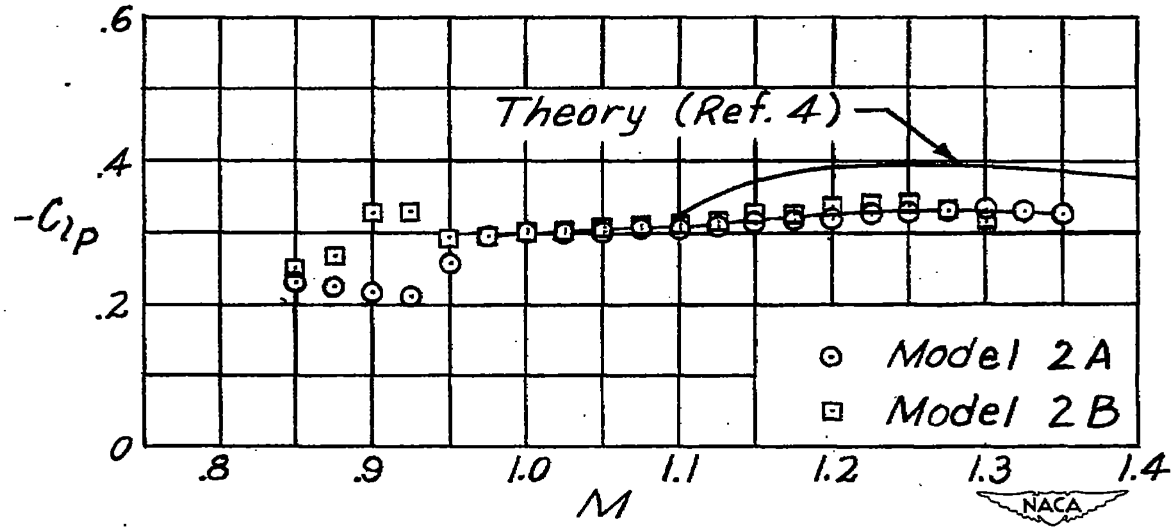

(b) Model 2; A = 3.0; $\frac{t}{c}$ = 0.09.

Figure 3.- Comparison of experimental C_{l_p} with theory from reference 4.

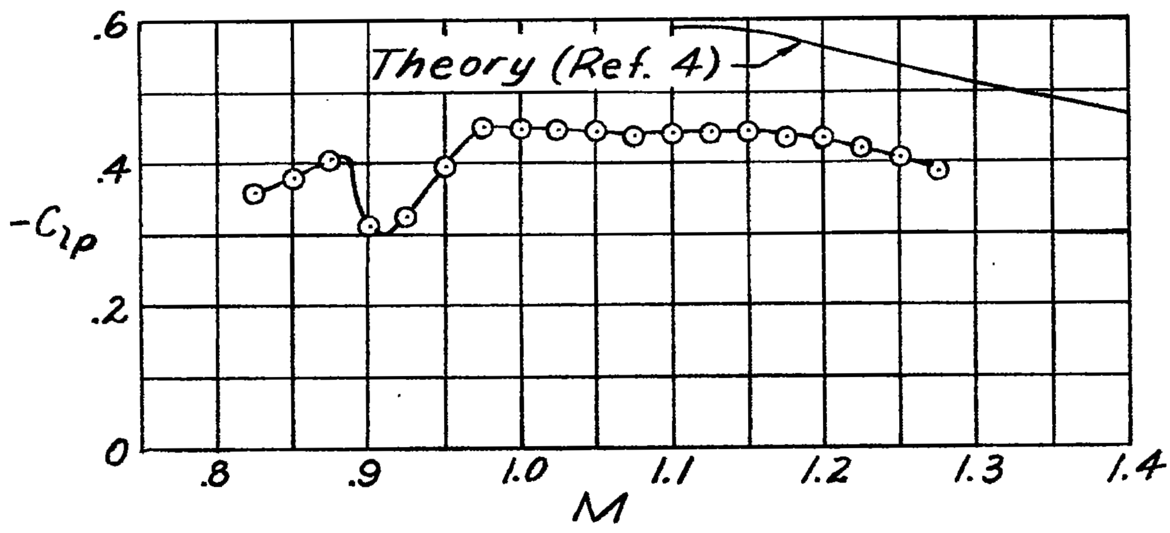

(c) Model 4; A = 4.5; $\frac{t}{c}$ = 0.09.

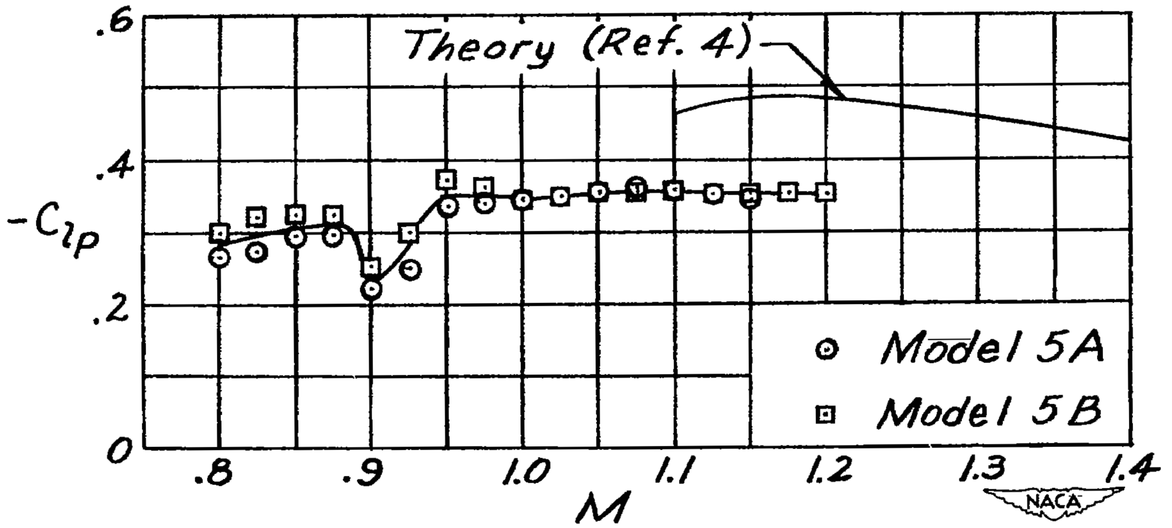

(d) Model 5; A = 3.7; $\frac{t}{c}$ = 0.12.

Figure 3.- Concluded.

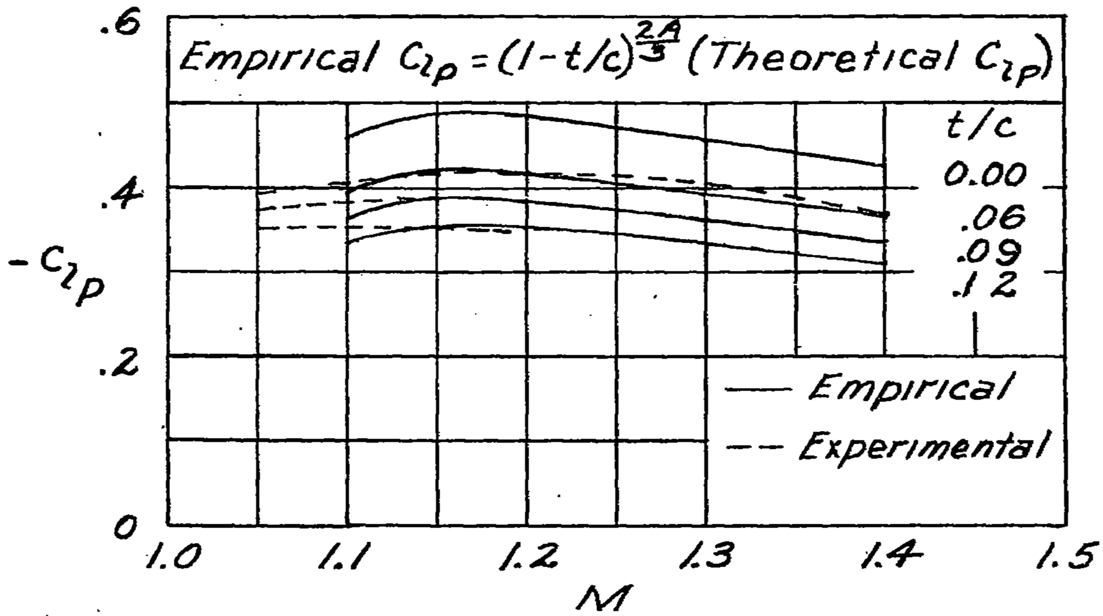

(a) Thickness-ratio series; A = 3.7.

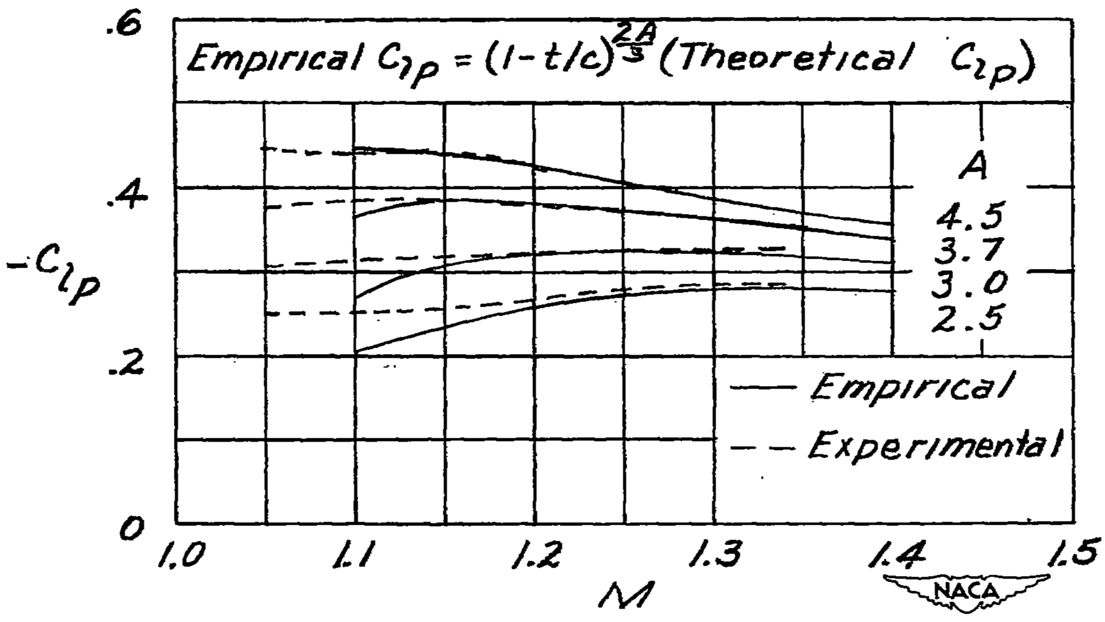

(b) Aspect-ratio series; $\frac{t}{c} = 0.09$.

Figure 4.- Comparison of experimental C_{l_p} with empirical C_{l_p}.

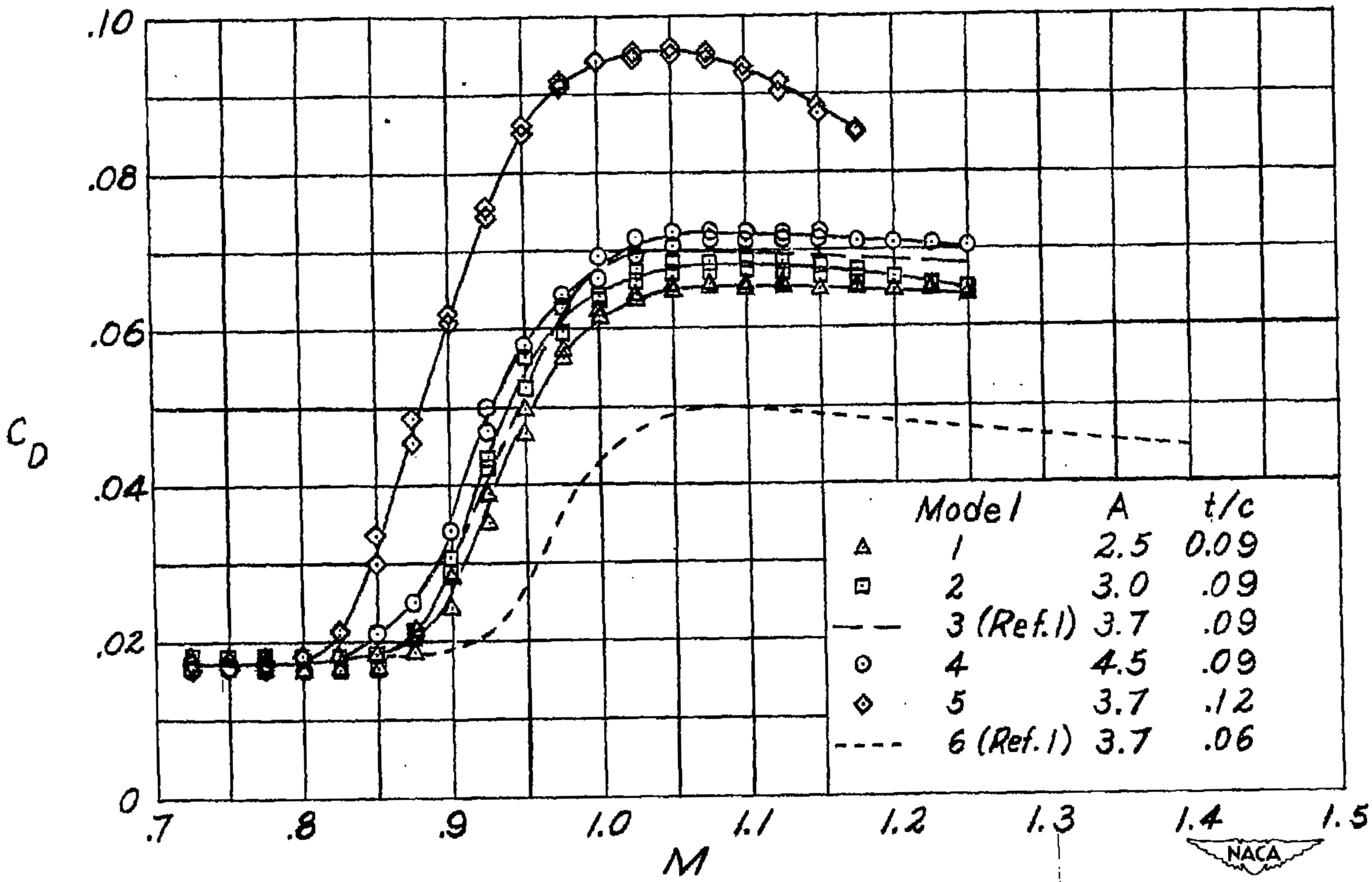

Figure 5.- Variation of total-drag coefficient with Mach number showing the effect of aspect ratio and thickness.